arXiv:1701.00786v1 [cond-mat.mes-hall] 3 Jan 2017

Universal Absence of Walker Breakdown and Linear Current–Velocity Relation *via* Spin–Orbit Torques in Coupled and Single Domain Wall Motion

Vetle Risinggård* and Jacob Linder
Department of Physics, NTNU, Norwegian University of Science and Technology, N-7491 Trondheim, Norway
(Dated: December 21, 2016)

We consider theoretically domain wall motion driven by spin–orbit and spin Hall torques. We find that it is possible to achieve universal absence of Walker breakdown for all spin–orbit torques using experimentally relevant spin–orbit coupling strengths. For spin–orbit torques other than the pure Rashba spin–orbit torque, this gives a linear current–velocity relation instead of a saturation of the velocity at high current densities. The effects is very robust and is found in both soft and hard magnetic materials, as well as in the presence of the Dzyaloshinskii–Moriya interaction and in coupled domain walls in synthetic antiferromagnets, where it leads to very high domain wall velocities.

Domain wall motion in ferromagnetic strips is a central theme in magnetization dynamics. The topic has fundamental interest, and has recently been instrumental to the discovery of several new current-induced effects on the magnetization dynamics [1–6]. Particularly since the proposal of racetrack memories [7]—made possible by current-induced torques—domain wall motion has also had a technological interest, motivating the search for ever higher domain wall velocities. The attainable velocity of a domain wall driven by conventional spin-transfer torques (STTs) is limited by the Walker breakdown [8], upon which the domain wall has a negative differential velocity with respect to the current.

Current-induced torques derived from spin–orbit effects (SOTs) such as an interfacial Rashba spin–orbit coupling [9–11] or the spin Hall effect [4–6, 12] have enabled large domain wall velocities. We consider the dependence of the domain wall velocity on the current and find that regardless of the relative importance of the reactive and dissipative components of the torque it is possible to achieve universal absence of Walker breakdown for all current densities for experimentally relevant spin–orbit coupling strengths. For spin–orbit torques other than the pure Rashba SOTs, such as the spin Hall torques, the velocity will not saturate as a function of current, but increase linearly as long as a conventional spin-transfer torque is present. This behavior is robust against the presence of an interfacial Dzyaloshinskii–Moriya interaction [13, 14] and is found both in perpendicular anisotropy ferromagnets and in shape anisotropy-dominated strips.

Very recently, domain wall dynamics in bilayer racetracks antiferromagnetically coupled by interlayer exchange has been considered both theoretically and experimentally [15–18]. We find that this system also exhibits universal absence of Walker breakdown and asymptotic linear dependence of the velocity on the current. The strength of the interlayer exchange coupling (IEC) determines the rate at which the velocity approaches the asymptotic solution. This enables very high domain wall velocities for relatively small current densities. The combination of SOTs with the interlayer exchange torque also enables other interesting effects such as a nonmonotonic dependence of the domain wall velocity on the ratio of the thicknesses of the ferromagnets.

Universal Absence of Walker Breakdown. We consider an ultrathin ferromagnet with a heavy metal underlayer as shown in Figure 1. We describe the dynamics of the magnetization $\boldsymbol{m}(\boldsymbol{r}, t)$ using the Landau–Lifshitz–Gilbert (LLG) equation [19, 20],

$$\partial_t \boldsymbol{m} = \gamma \boldsymbol{m} \times \boldsymbol{H} - \frac{\alpha}{m} \boldsymbol{m} \times \partial_t \boldsymbol{m} + \boldsymbol{\tau}, \tag{1}$$

where $\gamma < 0$ is the gyromagnetic ratio, m is the saturation magnetization, $\alpha < 0$ is the Gilbert damping, $\boldsymbol{H} = -\delta F/\delta \boldsymbol{m}$ is the effective field acting on the magnetization and $\boldsymbol{\tau}$ is the current-induced torques. The free energy F of the ferromagnet is a sum,

$$F = \int \mathrm{d}\boldsymbol{r} \left(f_{\mathrm{Z}} + f_{\mathrm{ex}} + f_{\mathrm{DM}} + f_{\mathrm{a}} \right), \tag{2}$$

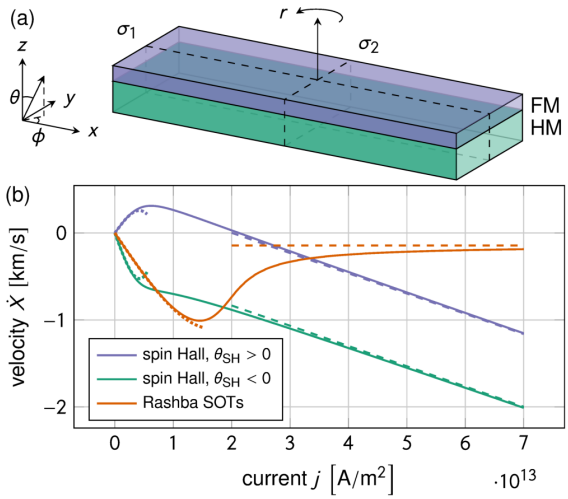

Figure 1. Domain wall dynamics in a single ferromagnet. (a) Ultrathin ferromagnet with a heavy metal underlayer. We consider transverse domain wall motion along the x axis. r, σ_1 and σ_s denote the three nontrivial operations of the symmetry group C_{2v}. (b) Current–velocity relation for three different SOTs. The Rashba SOTs level off to a constant velocity at large currents, whereas the spin Hall torques asymptotically approach a linear current–velocity relation. Dashed lines show the asymptotic expansion and dotted curves show the series about $j = 0$. We use $\gamma = -0.19\,\mathrm{GHz/T}$, $\lambda = 4\,\mathrm{nm}$, $K_y = 200\,\mathrm{kJ/m^3}$, $m = 1\,\mathrm{MA/m}$, $D = -1.4\,\mathrm{mJ/m^2}$, $\alpha = -0.25$, $\beta = 0.5$, $P = 0.5$, $H_x = 0$, $\alpha_{\mathrm{R}} = 6.3\,\mathrm{meV\,nm}$, $\theta_{\mathrm{SH}} = 0.1$, $\beta_{\mathrm{SH}} = 0.02$ and $t = 1.2\,\mathrm{nm}$.

of the Zeeman energy due to any applied magnetic fields, the isotropic exchange, the magnetic anisotropy and the interfacial Dzyaloshinskii–Moriya interaction.

The Zeeman energy and the isotropic exchange can be written respectively as [20] $f_{\rm Z} = -\boldsymbol{H}_0 \cdot \boldsymbol{m}$, where $\boldsymbol{H}_0$ is the applied magnetic field, and [20] $f_{\rm ex} = (A/m^2)[(\nabla m_x)^2 + (\nabla m_y)^2 + (\nabla m_z)^2]$, where A is the exchange stiffness. Inversion symmetry breaking at the interface between the heavy metal and the ferromagnet gives rise to an anisotropic contribution to the exchange known as the Dzyaloshinskii–Moriya interaction, which favors a canting of the spins [13, 14, 21]. The resulting contribution to the free energy is $f_{\rm DM} = (D/m^2)[m_z(\nabla \cdot \boldsymbol{m}) - (\boldsymbol{m} \cdot \nabla)m_z]$, where D is the magnitude of the Dzyaloshinskii–Moriya vector.

Ultrathin magnetic films are prone to exhibit perpendicular magnetization due to interface contributions to the magnetic anisotropy [22]. Consequently, we write the magnetic anisotropy energy as $f_{\rm a} = -K_z m_z^2 + K_y m_y^2$, corresponding to an easy axis in the z-direction and a hard axis in the y-direction.

The current-induced torques $\boldsymbol{\tau}$ are conventionally divided into spin-transfer torques [23–25],

$$\boldsymbol{\tau}_{\rm STT} = u\partial_x \boldsymbol{m} - \frac{\beta u}{m}\boldsymbol{m} \times \partial_x \boldsymbol{m}, \tag{3}$$

and spin–orbit torques [4–6, 9–12],

$$\boldsymbol{\tau}_{\rm R} = \gamma \boldsymbol{m} \times H_{\rm R}\boldsymbol{e}_y - \gamma \boldsymbol{m} \times \Big(\boldsymbol{m} \times \beta H_{\rm R}\boldsymbol{e}_y/m\Big), \tag{4}$$

$$\boldsymbol{\tau}_{\rm SH} = \gamma \boldsymbol{m} \times \Big(\boldsymbol{m} \times H_{\rm SH}\boldsymbol{e}_y/m\Big) + \gamma \boldsymbol{m} \times \beta_{\rm SH} H_{\rm SH}\boldsymbol{e}_y. \tag{5}$$

In fact, assuming that the stack can be described using the C_{2v} symmetry group as indicated by the symmetry operations in Figure 1(a), it can be shown that these torques exhaust the number of possible torque components if the current is only applied in the x direction and the width (y direction) and the thickness (z direction) of the ferromagnetic layer are so small that there is no magnetic texture along these axes (see Supplemental Material for details [26]).

There is one reactive and one dissipative spin-transfer torque, whose relative magnitude is parameterized by β [23–25]. The strength of the STTs is determined by the electric current j and its spin polarization P through $u = \mu_{\rm B} P j/[em(1+\beta^2)]$ where $\mu_{\rm B}$ is the Bohr magneton and e is the electron charge. The Rashba SOTs $\boldsymbol{\tau}_{\rm R}$ are due to the Rashba spin–orbit coupling induced in the ferromagnet by the broken inversion symmetry at the heavy metal interface [9–11]. Just as for the STTs, there is one reactive and one dissipative torque (β-term). The strength of the Rashba SOTs is determined by the Rashba spin–orbit coupling $\alpha_{\rm R}$ and the spin current through $H_{\rm R} = \alpha_{\rm R} P j/[2\mu_{\rm B} m(1+\beta^2)]$. The spin Hall torques $\boldsymbol{\tau}_{\rm SH}$ are due to the transversal spin current injected into the ferromagnet from the heavy metal due to the spin Hall effect [4–6, 12]. Since the polarization direction of this current changes sign upon time-reversal the principal spin Hall torque term is dissipative, while the $\beta_{\rm SH}$ correction is reactive. The magnitude of the spin Hall torques is determined by the injected spin current and the thickness of the ferromagnet t through $H_{\rm SH} = \hbar\theta_{\rm SH} j/(2emt)$.

As can be seen from the LLG equation (1), the magnitude m of the magnetization is constant, and the magnetization is conveniently parameterized in spherical coordinates as $\boldsymbol{m}/m = \cos\phi \sin\theta \boldsymbol{e}_x + \sin\phi \sin\theta \boldsymbol{e}_y + \cos\theta \boldsymbol{e}_z$. Using the assumption that there is no magnetic texture along the y and the z axes, giving $\nabla = \partial_x \boldsymbol{e}_x$, we can find the domain wall profile by minimizing the free energy or by solving the LLG equation (1) in the static limit, $\partial_t \boldsymbol{m} = 0$. If we assume that the azimuthal angle ϕ is independent of position, this gives the Néel wall solution $\theta = 2\arctan\exp[\pm(x-X)/\lambda]$ for the polar angle, where X is the domain wall position and $\lambda = \sqrt{A/K_z}$ is the domain wall width; and $\phi = n\pi$, where $n = 0, 2, 4, \ldots$ if $D < 0$ and we choose the + sign for θ, and $n = 1, 3, 5, \ldots$ if $D > 0$ and we choose the − sign for θ.

Substitution of this domain wall profile into the full LLG equation (1) using $\boldsymbol{H}_0 = H_x \boldsymbol{e}_x$ and a positive topological charge gives the collective coordinate equations,

$$\frac{\alpha \dot{X}}{\lambda} - \dot{\phi} = +\tfrac{\pi}{2}\gamma\Big(H_{\rm SH} - \beta H_{\rm R}\Big)\cos\phi + \frac{\beta u}{\lambda}, \tag{6}$$

$$(1+\alpha^2)\dot{\phi} = -\frac{\alpha\gamma K_y}{m}\sin 2\phi + \frac{\pi\alpha\gamma(D - H_x m\lambda)}{2m\lambda}\sin\phi \tag{7}$$
$$- \frac{u(\alpha+\beta)}{\lambda} - \tfrac{\pi}{2}\gamma\Big[H_{\rm SH}(1-\alpha\beta_{\rm SH}) - H_{\rm R}(\alpha+\beta)\Big]\cos\phi,$$

for the domain wall position X and tilt ϕ. The equations can be simplified by introducing $aj = \frac{\pi}{2}\gamma(H_{\rm SH} - \beta H_{\rm R})$, $bj = \beta u/\lambda$, $c = -2\alpha\gamma K_y/m$, $d = \pi\alpha\gamma(D - H_x m\lambda)/(2m\lambda)$, $ej = -\frac{\pi}{2}\gamma[H_{\rm SH}(1-\alpha\beta_{\rm SH}) - H_{\rm R}(\alpha+\beta)]$ and $fj = -u(\alpha+\beta)/\lambda$. Walker breakdown is absent when the time derivative $\dot{\phi}$ vanishes, resulting in the condition

$$0 = c\sin\phi\cos\phi + d\sin\phi + j(e\cos\phi + f). \tag{8}$$

If $e > f$ this equation will always have a solution for ϕ regardless of the value of j. For realistic material values this corresponds to a Rashba parameter $\alpha_{\rm R} > 4\mu_{\rm B}^2/(\pi e\gamma\lambda) = 5.5\,\text{meV nm}$ (pure Rashba SOTs) or a spin Hall angle $\theta_{\rm SH} > 4\mu_{\rm B} Pt/(\pi\hbar\gamma\lambda) = 0.091$ (pure spin Hall torques). The absence of Walker breakdown for sufficiently strong Rashba spin–orbit coupling has been pointed out previously [27], and can also be noted in references [10, 28–30].

Let us write $\xi = \cos\phi$ and $\eta = \sin\phi$, so that $\xi^2 + \eta^2 = 1$. Solving equation (8) for η to get $\eta = -j(e\xi + f)/(c\xi + d)$, this relation gives a quartic equation

$$\begin{aligned} c^2\xi^4 + 2cd\xi^3 + [(ej)^2 + d^2 - c^2]\xi^2 \\ + 2(efj^2 - cd)\xi + (fj)^2 - d^2 = 0. \end{aligned} \tag{9}$$

The exact solutions of the quartic (9) are hopelessly complicated. However, they all have the same series expansion around $j = 0$ and $j = \infty$. We consider first the asymptotic expansion, which gives

$$\xi = -\frac{f}{e} + \frac{S_1}{j} + O\left(j^{-2}\right), \tag{10}$$

where S_1 represents the solutions of the quadratic equation $e^6\zeta^2 = d^2e^4 + c^2f^4 + (c^2 - d^2)f^2e^2 + 2cdef(f^2 - e^2)$. The

domain wall velocity, as given by equation (6) then takes the form

$$\frac{\alpha \dot{X}}{\lambda} = bj - \frac{af}{e} j + aS_1 + aO\left(j^{-1}\right). \tag{11}$$

Back-substitution of the abbreviations a, b, f and e shows that for pure Rashba SOTs the coefficient of the linear term reduces to zero because the ratio of the reactive to the dissipative torque is the same for the STTs and the Rashba SOTs. Thus, for large j the domain wall velocity approaches a constant. Instead, for pure spin Hall torques we get the linear term $-u\alpha(1 + \beta\beta_{\mathrm{SH}})/[\lambda(1-\alpha\beta_{\mathrm{SH}})]$. This means that *for large j the velocity is actually independent of the sign of the spin Hall angle and increases linearly with j*. Note the importance of including the STTs—which are always present—in these considerations: in the absence of STTs ($u \to 0$) both b and f go to zero and the velocity levels off to a constant for large j for any combination of SOTs.

For completeness, we also consider the series expansion about $j = 0$, which gives $\xi = -1 + [(e - f)^2/2(c - d)^2]j^2 + O(j^4)$ and $\dot{X} = bj - aj + [a(e - f)^2/2(c - d)^2]j^3 + aO(j^5)$. The key observation here is that in this regime the velocity does depend on the sign of the spin Hall angle ($a \propto \theta_{\mathrm{SH}}$ for pure spin Hall torques) and increases with the cube of j. Figure 1(b) shows a numerical solution of the coupled equations (6) and (7) as a function of j for pure Rashba SOTs and for pure spin Hall torques both in the cases of $\theta_{\mathrm{SH}} > 0$ and $\theta_{\mathrm{SH}} < 0$ together with the analytical solutions close to $j = 0$ and for large j. We see that our analytical results successfully approximate the full solution in the expected ranges of validity (see Supplemental Material for a description of the numerics [26]).

The in-plane hard axis included in the magnetic anisotropy is appropriate for narrow ferromagnetic strips, which generally host Néel walls. Wider strips give Bloch walls [22], and by making the necessary modifications to the above calculations, we find that in this case the domain wall velocity retains the qualitative features elucidated above. This is also true for shape anisotropy-dominated strips, which host head-to-head walls. *This shows that universal absence of Walker breakdown is a robust effect that does not depend on the details of the ferromagnetic material*, unlike other SOT effects studied previously [31].

Coupled Domain Walls in a SAF Structure. We consider next an asymmetric stack of two ultrathin ferromagnets separated by an insulating spacer as shown in Figure 2(a). We describe the dynamics of each of the ferromagnets using separate LLG equations similarly to what was done in the previous section, but add to the free energy a coupling term,

$$F_{\mathrm{IEC}} = \int \frac{\mathrm{d}\boldsymbol{r}_1}{m^{(1)}} \int \frac{\mathrm{d}\boldsymbol{r}_2}{m^{(2)}} J(\boldsymbol{r}_1 - \boldsymbol{r}_2) \left[\boldsymbol{m}^{(1)}(\boldsymbol{r}_1) \cdot \boldsymbol{m}^{(2)}(\boldsymbol{r}_2)\right], \tag{12}$$

representing the interlayer exchange (IEC). We assume that the IEC is local in the plane, $J(\boldsymbol{r}_1 - \boldsymbol{r}_2) = J\delta(x_1 - x_2)\delta(y_1 - y_2)$. Equation (12) then represent the lowest order coupling proposed by Bruno [32]. The static solution will now depend on the signs of the Dzyaloshinskii–Moriya interactions in the two ferromagnets, as well as on their strength relative to the interlayer exchange and on the relative thickness of the ferromagnets. To limit the scope of the treatment we consider only the case where D_1 and D_2 have the same sign. Thus, for opposite topological charges for the two walls, both the DMI and the IEC favor the same chiralities for the walls.

Following the same procedure as in the previous section we may now derive four coupled collective coordinate equations (see Supplemental Material [26]). We solve these equations numerically for $t_1/t_2 = 1$ in the presence of STTs only and in the presence of spin Hall torques to get the current–velocity

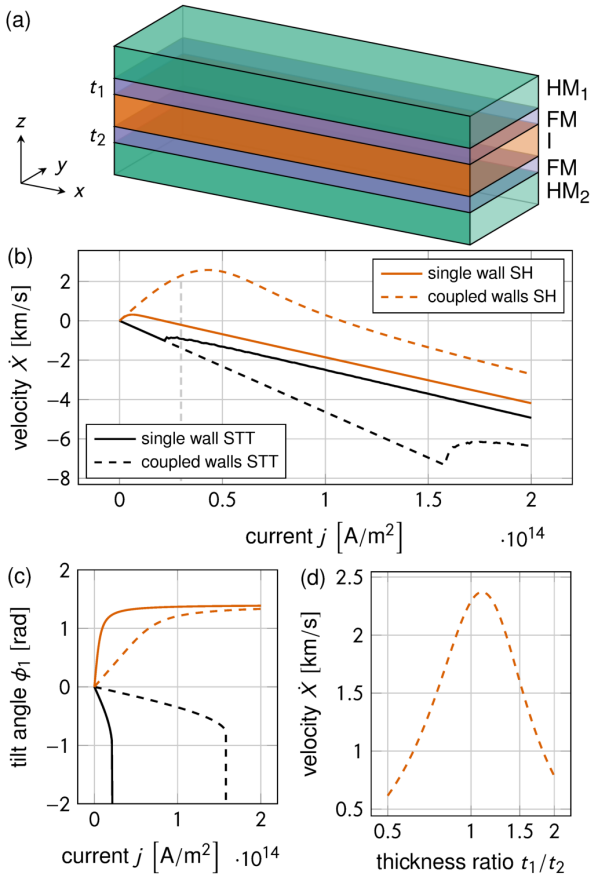

Figure 2. Domain wall dynamics in interlayer exchange coupled ferromagnets. (a) Two ultrathin ferromagnets separated by an insulating spacer with heavy metal over- and underlayers. The ferromagnets are identical except for their thicknesses, but the different heavy metals induce different DMI and SOTs. (b) and (c): Domain wall dynamics in single ferromagnets compared with a SAF structure. Black curves correspond to walls driven by STTs only, while orange curves include spin Hall torques. (b) The IEC delays Walker breakdown for STT-driving. With spin Hall torques there is universal absence of Walker breakdown and the IEC rescales the current axis. Both the results for STTs and spin Hall torques are the result of a suppression of the tilt angle as shown in (c). (d) The IEC gives the velocity a nonmonotonic thickness-dependence resulting in a peak close to $t_1/t_2 = 1$. Results in (d) are shown for $j = 3 \cdot 10^{13}\,\mathrm{A/m^2}$, corresponding to the dashed vertical line in (b). We use the same parameters as in Figure 1 with $t_2 = t_1 = 1.2\,\mathrm{nm}$ (except in (d) where t_2 is varied) and $J = (5\,\mathrm{mJ/m^2})/t_1 t_2$.

relations shown in Figure 2(b). We see that the presence of the IEC delays Walker breakdown when the wall is driven by ordinary STTs, but the subcritical differential velocity remains unaffected. This can also be shown analytically by solving for the tilt angle of the wall as a function of current. Such a calculation shows that the tilt angle is suppressed by the IEC (but the breakdown angle is still $\pi/4$). Back-substitution of this angle into the torque acting on the wall shows that this torque is independent of J, explaining that there is no change in the differential velocity.

A very similar mechanism emerges from the spin Hall torque results, which show that the main effect of the IEC is to rescale the current axis. Such a rescaling of the current can be understood in terms of the expansion (10) simply as a rescaling of the constant S_1 and the higher order constants $S_2, S_3, \ldots$ Again this is nothing but a suppression of the tilt angle, as seen in Figure 2(c). *This shows that universal absence of Walker breakdown is also found in SAF structures.* We note in particular that the combination of spin Hall torques and IEC produces much higher domain wall velocities than in single ferromagnets for comparatively small current densities.

In the case of a single ferromagnetic layer the velocity of a domain wall driven by spin Hall torques has a monotonic $1/t$ thickness dependence. As shown in Figure 2(d) the velocity of coupled walls in a SAF structure peaks close to $t_1/t_2 = 1$ when changing the thickness of layer 2 from $t_2 = 2t_1$ to $t_2 = t_1/2$. This peak is the result of two competing mechanisms. When t_2 is large the wall in layer 2 moves slower than the wall in layer 1 and the effective field felt by layer 1 due to the IEC—which is proportional to t_2—-is large. Thus the velocity of the double wall system is determined by wall 2. The velocity increases up to $t_1/t_2 \approx 1$ (the deviation from 1 is due to the DMI) following approximately the $1/t$ increase expected by a single wall. As the thickness changes further, $(\phi_1 - \phi_2)$ approaches π. As can be seen from equation (12) the IEC torque vanishes when the two magnetizations are colinear, and the velocity decreases towards the single wall value.

Conclusion. We have shown that complete suppression of Walker breakdown is possible in a wide range of domain wall systems driven by spin–orbit torques, including head-to-head walls in soft magnets, Bloch and Néel walls in PMA magnets, in the presence of the DMI and in coupled domain walls in SAFs. For SOTs other than pure Rashba SOTs this leads to a linear current–velocity relation instead of a saturation of the velocity for large currents. In combination with IEC, SOT-driven domain wall motion in SAFs gives rise to very high domain wall velocities.

Funding via the "Outstanding Academic Fellows" program at NTNU, the COST Action MP-1201, the NT-Faculty, and the Research Council of Norway Grant numbers 216700 and 240806, is gratefully acknowledged. We thank Morten Amundsen for very useful discussions of the numerics.

* vetle.k.risinggard@ntnu.no

[1] I. M. Miron, P.-J. Zermatten, G. Gaudin, S. Auffret, B. Rodmacq, and A. Schuhl, Phys. Rev. Lett. **102**, 137202 (2009).
[2] I. M. Miron, G. Gaudin, S. Auffret, B. Rodmacq, A. Schuhl, S. Pizzini, J. Vogel, and P. Gambardella, Nat. Mater. **9**, 230 (2010).
[3] I. M. Miron, T. Moore, H. Szambolics, L. D. Buda-Prejbeanu, S. Auffret, B. Rodmacq, S. Pizzini, J. Vogel, M. Bonfim, A. Schuhl, and G. Gaudin, Nat. Mater. **10**, 419 (2011).
[4] S. Emori, U. Bauer, S.-M. Ahn, E. Martinez, and G. S. D. Beach, Nat. Mater. **12**, 611 (2013).
[5] K.-S. Ryu, L. Thomas, S.-H. Yang, and S. Parkin, Nat. Nanotechnol. **8**, 527 (2013).
[6] P. P. J. Haazen, E. Murè, J. H. Franken, R. Lavrijsen, H. J. M. Swagten, and B. Koopmans, Nat. Mater. **12**, 299 (2013).
[7] S. S. P. Parkin, M. Hayashi, and L. Thomas, Science **320**, 190 (2008).
[8] N. L. Schryer and L. R. Walker, J. Appl. Phys. **45**, 5406 (1974).
[9] A. Manchon and S. Zhang, Phys. Rev. B **78**, 212405 (2008).
[10] K.-W. Kim, S.-M. Seo, J. Ryu, K.-J. Lee, and H.-W. Lee, Phys. Rev. B **85**, 180404 (2012).
[11] A. Chernyshov, M. Overby, X. Liu, J. K. Furdyna, Y. Lyanda-Geller, and L. P. Rokhinson, Nat. Phys. **5**, 656 (2009).
[12] K. Ando, S. Takahashi, K. Harii, K. Sasage, J. Ieda, S. Maekawa, and E. Saitoh, Phys. Rev. Lett. **101**, 036601 (2008).
[13] I. E. Dzyaloshinskii, J. Exp. Theor. Phys. **5**, 1259 (1957).
[14] T. Moriya, Phys. Rev. Lett. **4**, 228 (1960); Phys. Rev. **120**, 91 (1960).
[15] H. Saarikoski, H. Kohno, C. H. Marrows, and G. Tatara, Phys. Rev. B **90**, 094411 (2014).
[16] S. Lepadatu, H. Saarikoski, R. Beacham, M. J. Benitez, T. A. Moore, G. Burnell, S. Sugimoto, D. Yesudas, M. C. Wheeler, J. Miguel, S. S. Dhesi, D. McGrouther, S. McVitie, G. Tatara, and C. H. Marrows, arXiv:1604.07992.
[17] S.-H. Yang, K.-S. Ryu, and S. Parkin, Nat. Nanotechnol. **10**, 221 (2015).
[18] R. Tomasello, V. Puliafito, E. Martinez, A. Manchon, M. Ricci, M. Carpentieri, and G. Finocchio, arXiv:1610.00894.
[19] L. D. Landau and E. M. Lifshitz, Phys. Zeitschrift der Sowjetunion **8**, 153 (1935); Ukr. J. Phys. **53**, 14 (2008).
[20] T. Gilbert, IEEE Trans. Magn. **40**, 3443 (2004).
[21] A. Fert, Mater. Sci. Forum **59–60**, 439 (1990).
[22] R. C. O'Handley, *Modern magnetic materials. Principles and applications* (John Wiley & Sons, 2000).
[23] S. Zhang and Z. Li, Phys. Rev. Lett. **93**, 127204 (2004).
[24] G. Beach, M. Tsoi, and J. Erskine, J. Magn. Magn. Mater. **320**, 1272 (2008).
[25] A. Brataas, A. D. Kent, and H. Ohno, Nat. Mater. **11**, 372 (2012).
[26] See Supplemental Material, which includes Refs. [32–38], for details on the possible spin–orbit torques in this system, a description of the numerics and for the collective coordinate equations for the coupled domain walls.
[27] J. Linder and M. Alidoust, Phys. Rev. B **88**, 064420 (2013).
[28] M. Stier, M. Creutzburg, and M. Thorwart, Phys. Rev. B **90**, 014433 (2014).
[29] O. Boulle, L. D. Buda-Prejbeanu, E. Jué, I. M. Miron, and G. Gaudin, J. Appl. Phys. **115**, 17D502 (2014).
[30] P.-B. He, H. Yan, M.-Q. Cai, and Z.-D. Li, Europhys. Lett. **114**, 67001 (2016).
[31] A. V. Khvalkovskiy, V. Cros, D. Apalkov, V. Nikitin, M. Krounbi,

K. A. Zvezdin, A. Anane, J. Grollier, and A. Fert, Phys. Rev. B **87**, 020402 (2013).
[32] P. Bruno, Phys. Rev. B **52**, 411 (1995).
[33] K. M. D. Hals and A. Brataas, Phys. Rev. B **88**, 085423 (2013); Phys. Rev. B **91**, 214401 (2015).
[34] R. R. Birss, *Symmetry and Magnetism*, 1st ed., edited by E. P. Wohlfarth, Selected Topics in Solid State Physics, Vol. 3 (North-Holland Publising Company, 1964).
[35] J. Kim, J. Sinha, M. Hayashi, M. Yamanouchi, S. Fukami, T. Suzuki, S. Mitani, and H. Ohno, Nat. Mater. **12**, 240 (2012).
[36] K.-S. Ryu, S.-H. Yang, L. Thomas, and S. S. P. Parkin, Nat. Commun. **5**, 3910 (2014).
[37] X. Fan, H. Celik, J. Wu, C. Ni, K.-J. Lee, V. O. Lorenz, and J. Q. Xiao, Nat. Commun. **5**, 3042 (2014).
[38] J. R. Dormand and P. J. Prince, J. Comput. Appl. Math. **6**, 19 (1980).

Supplemental Material for Universal Absence of Walker Breakdown and Linear Current–Velocity Relation *via* Spin–Orbit Torques in Coupled and Single Domain Wall Motion

Vetle Risinggård and Jacob Linder
Department of Physics, NTNU, Norwegian University of Science and Technology, N-7491 Trondheim, Norway
(Dated: December 21, 2016)

SYMMETRY ADMISSIBLE SPIN–ORBIT TORQUES

Hals and Brataas [S1] describe spin–orbit torques and generalized spin-transfer torques in terms of a tensor expansion. Assuming the lowest orders are sufficient to describe the essential dynamics, the reactive and dissipative spin–orbit torques are described by respectively an axial second rank tensor and a polar third rank tensor while the generalized spin-transfer torques are described using a polar fourth rank tensor and an axial fifth rank tensor. The torques that arise in a given structure are limited by the requirement that the tensors must be invariant under the symmetry operations fulfilled by the structure. We have assumed that the physical systems we consider are described by C_{2v} symmetry. Combined with the fact that the current is applied in the x direction only and that $\partial_y \boldsymbol{m} = 0$ and $\partial_z \boldsymbol{m} = 0$, this implies that there are only 1 relevant nonzero element in the axial second rank tensor, 2 elements in the polar third rank tensor, 3 elements in the polar fourth rank tensor and 6 elements in the axial fifth rank tensor [S2].

The 3 relevant nonzero elements of the second and third rank tensors give rise to 3 spin–orbit torques. A detailed analysis shows that these torque components are captured by the Rashba and spin Hall torques in equations (4) and (5) in the main text. As an aside, we note that although the Rashba and spin Hall effects may not necessarily capture all of the relevant microscopic physics [S3–S5] these torques can still be used to model the dynamics because they contain 3 'free' parameters, α_{R}, θ_{SH} and β_{SH}.

As has been shown by Hals and Brataas [S1], the generalized spin-transfer torques reduce to the ordinary STTs in the nonrelativistic limit. Thus, by using the ordinary STTs we neglect possible spin–orbit coupling corrections to these higher order terms.

EQUATIONS OF MOTION FOR SAF STRUCTURE

We assume that the interlayer exchange coupling (IEC) is completely local in the plane [S6], $J(\boldsymbol{r}_1 - \boldsymbol{r}_2) = J\delta(x_1 - x_2)\delta(y_1 - y_2)$. It follows that the IEC should not affect the domain wall profile, but can only determine the chirality of coupled domain walls. Thus, we can use the static solution derived in the main text, $\theta = 2\arctan\exp[\pm(x - X)/\lambda]$, where $\lambda = \sqrt{A/K_z}$ is the domain wall width. For a single wall the azimuthal angle ϕ is given by $\phi = n\pi$, where $n = 0, 2, 4, \ldots$ if $D < 0$ and we choose the + sign for θ, and $n = 1, 3, 5, \ldots$ if $D > 0$ and we choose the − sign for θ. Two coupled walls must have opposite topological charges. If D_1 and D_2 both are negative the DMI and the IEC cooperate to give the static solution $\phi_1 = 0$ (positive topological charge) and $\phi_2 = \pi$ (negative topological charge).

Substituting this static solution into the LLG equation using $\boldsymbol{H}_0 = H_x \boldsymbol{e}_x$ gives the collective coordinate equations

$$\begin{aligned}(1+\alpha^2)\frac{\dot{X}_1}{\lambda} =& -\frac{\gamma K_y}{m}\sin 2\phi_1 + \frac{\pi\gamma(D_1 - H_x m\lambda)}{2m\lambda}\sin\phi_1 + \frac{\gamma J t_2}{2m}\Big[\alpha U(s)\cos(\phi_1-\phi_2) + \alpha W(s) + V(s)\sin(\phi_1-\phi_2)\Big] \\ & - \frac{u(1-\alpha\beta)}{\lambda} + \tfrac{\pi}{2}\gamma\Big[H_{\mathrm{SH}}^{(1)}\big(\alpha + \beta_{\mathrm{SH}}^{(1)}\big) + H_{\mathrm{R}}^{(1)}(1-\alpha\beta)\Big]\cos\phi_1,\end{aligned} \tag{S1}$$

$$\begin{aligned}(1+\alpha^2)\frac{\dot{X}_2}{\lambda} =& +\frac{\gamma K_y}{m}\sin 2\phi_2 + \frac{\pi\gamma(D_2 + H_x m\lambda)}{2m\lambda}\sin\phi_2 - \frac{\gamma J t_1}{2m}\Big[\alpha U(s)\cos(\phi_1-\phi_2) + \alpha W(s) - V(s)\sin(\phi_1-\phi_2)\Big] \\ & - \frac{u(1-\alpha\beta)}{\lambda} + \tfrac{\pi}{2}\gamma\Big[H_{\mathrm{SH}}^{(2)}\big(\alpha + \beta_{\mathrm{SH}}^{(2)}\big) + H_{\mathrm{R}}^{(2)}(1-\alpha\beta)\Big]\cos\phi_2,\end{aligned} \tag{S2}$$

$$\begin{aligned}(1+\alpha^2)\dot{\phi}_1 =& -\frac{\alpha\gamma K_y}{m}\sin 2\phi_1 + \frac{\pi\alpha\gamma(D_1 - H_x m\lambda)}{2m\lambda}\sin\phi_1 - \frac{\gamma J t_2}{2m}\Big[U(s)\cos(\phi_1-\phi_2) + W(s) - \alpha V(s)\sin(\phi_1-\phi_2)\Big] \\ & - \frac{u(\alpha+\beta)}{\lambda} - \tfrac{\pi}{2}\alpha\gamma\Big[H_{\mathrm{SH}}^{(1)}\big(1 - \alpha\beta_{\mathrm{SH}}^{(1)}\big) - H_{\mathrm{R}}^{(1)}(\alpha+\beta)\Big]\cos\phi_1,\end{aligned} \tag{S3}$$

$$(1+\alpha^2)\dot{\phi}_2 = -\frac{\alpha\gamma K_y}{m}\sin 2\phi_2 - \frac{\pi\alpha\gamma(D_2+H_x m\lambda)}{2m\lambda}\sin\phi_2 - \frac{\gamma J t_1}{2m}\Big[U(s)\cos(\phi_1-\phi_2)+W(s)+\alpha V(s)\sin(\phi_1-\phi_2)\Big] + \frac{u(\alpha+\beta)}{\lambda} + \tfrac{\pi}{2}\alpha\gamma\Big[H^{(2)}_{\mathrm{SH}}\big(1-\alpha\beta^{(2)}_{\mathrm{SH}}\big) - H^{(2)}_{\mathrm{R}}(\alpha+\beta)\Big]\cos\phi_2. \tag{S4}$$

where we have assumed that the bulk parameters of the two ferromagnets are equal and where s is the separation between the two walls, $s = (X_1 - X_2)/\lambda$. The IEC terms are expressed using the three functions $V(s)$, $U(s)$ and $W(s)$: $V(s) = 4se^s/(e^{2s}-1)$, $U(s) = -4e^s(e^{2s}(s-1)+s+1)/(e^{2s}-1)^2$ and $W(s) = 2(e^{4s}-4se^{2s}-1)/(e^{2s}-1)^2$. These functions are plotted in Figure 1.

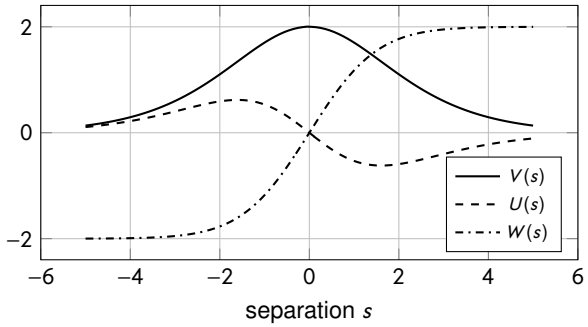

Figure 1. Dependence of the IEC terms on the domain wall separation.

Table I. Material parameters used for the numerical solution of equations (S1) through (S4) and for analytical estimates in the main text.

parameter	value	unit
gyromagnetic ratio γ	0.19	GHz/T
domain wall width λ	4.0	nm
hard axis anisotropy K_y	0.20	MJ/m^3
saturation magnetization m	1.0	MA/m
Dzyaloshinskii–Moriya const. D	−1.4	mJ/m^2
Gilbert damping α	0.25	
spin-polarization P	0.50	
nonadiabacity parameter β	0.50	
Rashba spin–orbit coupling α_{R}	6.3	meVnm
spin Hall angle θ_{SH}	0.1	
spin Hall β-term β_{SH}	0.02	
interlayer exchange Jt_1t_2	5.0	mJ/m^2
thickness t	1.2	nm

NUMERICS

Equations (S1) and (S3) reduce to equations (6) and (7) in the main text when $J \to 0$. To solve equations (S1) through (S4) numerically, we rescale the equations to obtain dimensionless variables. The dimension of equations (S1) through (S4) is Hz. A convenient scaling factor with the same dimensions is $\mu_0\gamma m$. By dividing equations (S1) through (S4) by $\mu_0\gamma m$ we get the rescaled variables $\tilde{t} = t\mu_0\gamma m$, $\tilde{X}_i = X_i/\lambda$, $\tilde{H}_x = H_x/\mu_0 m$, $\tilde{K}_y = K_y/\mu_0 m^2$, $\tilde{D}_i = D_i/\mu_0 m^2\lambda$, $\tilde{t}_i = t_i/\lambda$, $\tilde{J} = J\lambda/\mu_0 m^2$ and $\tilde{u} = u/\mu_0\gamma m\lambda$.

Equations (S1) through (S4) are solved using an explicit fourth order Runge–Kutta scheme with adaptive stepsize control, implemented as a Dormand–Prince pair [S7]. Material parameters are chosen to match approximately Co or Co/Ni multilayers, see Table I.

[S1] K. M. D. Hals and A. Brataas, Physical Review B **88**, 085423 (2013); Physical Review B **91**, 214401 (2015).

[S2] R. R. Birss, *Symmetry and Magnetism*, 1st ed., edited by E. P. Wohlfarth, Selected Topics in Solid State Physics, Vol. 3 (North-Holland Publising Company, 1964).

[S3] J. Kim, J. Sinha, M. Hayashi, M. Yamanouchi, S. Fukami, T. Suzuki, S. Mitani, and H. Ohno, Nature Materials **12**, 240 (2012).

[S4] K.-S. Ryu, S.-H. Yang, L. Thomas, and S. S. P. Parkin, Nature Communications **5**, 3910 (2014).

[S5] X. Fan, H. Celik, J. Wu, C. Ni, K.-J. Lee, V. O. Lorenz, and J. Q. Xiao, Nature Communications **5**, 3042 (2014).

[S6] P. Bruno, Physical Review B **52**, 411 (1995).

[S7] J. R. Dormand and P. J. Prince, Journal of Computational and Applied Mathematics **6**, 19 (1980).